

FABRICATION OF Mg-Zn-Al HYDROTALCITE AND ITS APPLICATION FOR Pb²⁺ REMOVAL

EDDY HERALDY^{a,b,*}, FITRIA RAHMAWATI^{a,b}, DWI ARDIYANTI^a,
IKA NURMAWANTI^a

^a *Sebelas Maret University, Faculty of Mathematics and Natural Sciences, Department of Chemistry, Jl. Ir. A. Sutami 36A, Kentingan, Surakarta 57126, Indonesia*

^b *Sebelas Maret University, Chemistry Department, Solid State Chemistry and Catalyst Research Group, Jl. Ir. A. Sutami 36A, Kentingan, Surakarta 57126, Indonesia*

* corresponding author: eheraldymipa.uns.ac.id

ABSTRACT. The fabrication of Mg-Zn-Al Hydrotalcite (HT) was carried out by the co-precipitation method at various molar ratios. The Mg-Zn-Al HT compound at the optimum molar ratio was then calcined to determine the effect of calcination on the Pb²⁺ adsorption. The kinetics of the adsorption type was determined by applying pseudo first order and pseudo second order kinetics models. Meanwhile, to investigate the adsorption process, the Freundlich and Langmuir equations were applied to determine the adsorption isotherm. The results showed that the optimum Mg-Zn-Al HT was at a molar ratio of 3 : 1 : 1 with an adsorption efficiency of 73.16 %, while Mg-Zn-Al HT oxide increased the adsorption efficiency to 98.12 %. The optimum condition of Pb²⁺ removal using Mg-Zn-Al HT oxide was reached at pH 5 and a contact time of 30 minutes. The adsorption kinetics follows the pseudo second order kinetics model with a rate constant of 0.544 g/mg·min. The isotherm adsorption follows the Langmuir isotherm model with a maximum capacity of 3.916 mg/g and adsorption energy of 28.756 kJ/mol.

KEYWORDS: Adsorption, isotherm, kinetics, Mg-Zn-Al hydrotalcite, Pb²⁺ removal.

1. INTRODUCTION

Hydrotalcite compounds (HT), which are also known as Layered Double Hydroxides (LDH) or anionic clays, are layered materials that have an anion exchange capacity and a large surface area [1–4]. The HT compounds have a general formula: $[M(II)_{1-x}M(III)_x(OH)_2]_x^{+}(An)_x/n \cdot mH_2O$; in which, M(II) is a divalent metal cation, and M(III) is a trivalent metal cation. The An⁻ is a balancing anion with x as the molar ratio fraction and m as the number of water molecules in the interlayer [1, 5]. The replacement of several M(II) by M(III) cations in the HT structure causes the hydroxide layer to be of an excess positive charge. The excess positive charge is balanced by an interlayer consisting of anions and water molecules [6–8].

Some researchers applied the HT for a metal cation adsorption including an adsorption of In³⁺ by Zn-Al LDH [9], adsorption of Cr⁶⁺ using Mg-Al LDH, Ni-Al LDH and Zn-Al LDH [10]. Adsorption of Cu²⁺ by Ca-Al-Zn LDH oxide [11], and Pb²⁺ adsorption using LDH Co-Mo [12]. The previous study shows that the HT is a potential adsorbent for Pb²⁺, even though the HTs also bear a positive charge on the hydroxide layer. The positive charge on the surface of the HT will interact with hydroxide ions in the solution that forms metal hydroxide on the HT surface [9]. In addition, a calcination treatment at 400–500 °C can convert the HT to a metal oxide [13]. If the metal oxide is dispersed into water, it will re-construct the

HT layered structure. This is named as the memory effects. This unique character causes the HT to be widely used as adsorbent, such as namely for heavy metal pollutants [3, 5].

The heavy metal pollution is dangerous for the human health [14–16]. The Pb²⁺ ion is a kind of heavy metals frequently found in liquid waste [3]. Due to the negative impacts of lead, therefore, the presence of lead in the environment must comply with regulations. Several methods have been applied to reduce the lead metal content from in a liquid waste, such as precipitation method, ion exchange, electrolysis, membrane filtration, and adsorption [17, 18]. The adsorption method is considered, as the most effective method due to lesser cost required. In addition, the absorption capacity is higher, the process is simple, and the efficiency is relatively high and does not provide side effects in the form of toxic substances [19]. Numerous adsorbents, for example, tourmaline, biosorbent, montmorillonite, activated carbon, zeolite, waste biomass, wheat straw, black phosphorous nanosheet, and Sulfur-doped Graphitic Carbon Nitride had been reported [20–28].

Therefore, the current study focused on a synthesis of Mg-Zn-Al HT by a co-precipitation method and their possibility as an effective and economical adsorbent for the Pb²⁺ ion removal. The variable operating parameters such as the pH of a solution, initial concentration of lead ions, and contact time were examined. As the profile of adsorption equilibrium, was used the Langmuir and Freundlich isotherm

was used. The adsorption behaviour occasionally was occasionally studied by kinetics studies.

2. MATERIAL AND METHODS

2.1. MATERIALS

Some materials for the Mg-Zn-Al HT synthesis were $\text{Mg}(\text{NO}_3)_2 \cdot 6\text{H}_2\text{O}$, $\text{Al}(\text{NO}_3)_3 \cdot 9\text{H}_2\text{O}$, $\text{Zn}(\text{NO}_3)_2 \cdot 4\text{H}_2\text{O}$, K_2CO_3 , KOH , HNO_3 and $\text{Pb}(\text{NO}_3)_2$ standard solution. All chemical reagents are analytical grade and were procured from Merck, Indonesia. All were used without any further purification.

2.2. PROCEDURE

2.2.1. FABRICATION OF Mg-Zn-Al HT

ADSORBENTS

The Mg-Zn-Al HT was fabricated from $\text{Mg}(\text{NO}_3)_2 \cdot 6\text{H}_2\text{O}$, $\text{Al}(\text{NO}_3)_3 \cdot 9\text{H}_2\text{O}$ and $\text{Zn}(\text{NO}_3)_2 \cdot 4\text{H}_2\text{O}$ by the co-precipitation method in an alkaline media at a constant pH [29]. The molar ratios of Mg:Zn:Al were 4 : 0 : 1, 3 : 1 : 1, 2 : 2 : 1 and 1 : 3 : 1. Based on the molar ratio, all chemicals were dissolved in 200 mL of distilled water. The K_2CO_3 and KOH were then added until the pH reached 10. The mixture was then distilled at 80 °C for 4 h. The precipitate formed was washed with water until the pH reached 7, and then it was dried at 100 °C for 24 h. The prepared powder was then heated at 450 °C for 5 h to produce the oxide of Mg-Zn-Al-HT.

2.2.2. BATCH ADSORPTION EXPERIMENTS DESIGN

Batch adsorption experiments were performed in a series of 250 mL conical flask containing 25 mL of $\text{Pb}(\text{NO}_3)_2$ solution. This solution was prepared to study the effect of the contact time (15, 30, 60, 90 and 120 min); pH (3, 4, 5, and 6); and the initial Pb^{2+} concentration (10, 20, 30, 40 and 50 ppm) at 120 rpm. After the adsorption had finished, the solution was filtered and the filtrate was analysed by an atomic absorption spectrophotometer (AAS). The Pb^{2+} adsorption efficiency was calculated by the equation (1) [20, 30, 31]:

$$\text{Adsorption efficiency (\%)} = \left\{ \frac{C_0 - C_e}{C_0} \right\} \times 100 \% \quad (1)$$

The C_0 and C_e are the initial concentrations of Pb^{2+} (mg/L) at $t = 0$ and the equilibrium concentration, respectively. The adsorption capacity (q) was calculated by a mass balance equation of adsorbent as depicted in equation:

$$q = \frac{(C_0 - C_e)V}{W} \quad (2)$$

In which, V is the volume of the Pb^{2+} solution (L), and W is the mass of the adsorbent (g).

ADSORBENTS OPTIMIZATION

The adsorbents optimization was carried out by 0.05 g adsorbent with a various Mg:Zn:Al molar ratio of 4 : 0 : 1, 3 : 1 : 1, 2 : 2 : 1, and 1 : 3 : 1 with 10 mL of Pb^{2+} 5 ppm solution. The adsorption was performed for 2 h at 120 rpm speed. The remaining Pb^{2+} was analysed by AAS.

ADSORBENTS EFFECTIVENESS TEST

0.05 g of the prepared Mg-Zn-Al-HT adsorbent was added to 10 mL of the Pb^{2+} 5 ppm solution. The mixture was stirred with a rotary shaker for 2 h at 120 rpm. The remaining Pb^{2+} in the solution was analysed by the AAS.

THE EFFECT OF PH SOLUTION

The effect of the pH solution to the Pb^{2+} removal was investigated by conducting an adsorption experiment under various pH values of 3, 4, 5 and 6. A define amount of adsorbent was mixed with a 5 ppm Pb^{2+} solution and then, it was agitated for 2 h at a room temperature. The remaining Pb^{2+} in solution was analysed by the AAS.

THE EFFECT OF CONTACT TIME

The adsorption process was conducted under various contact times 15, 30, 60, 90, and 120 min at the optimum pH. The Pb^{2+} concentration was 5 ppm. Thereafter, samples were filtered and the Pb^{2+} content in the filtrate was determined using the AAS.

THE EFFECT OF Pb^{2+} ION CONCENTRATION

In order to investigate the effect of the Pb^{2+} concentration, an adsorption experiment was conducted under the optimum pH for 120 min. The experiment used various Pb^{2+} initial concentrations, i.e., 5, 10, 20, 30, 40 and 50 ppm. The adsorption result was then filtered and the Pb^{2+} content in the filtrate was analysed by the AAS.

3. RESULTS AND DISCUSSION

3.1. CHARACTERIZATION OF Mg-Zn-Al HT

3.1.1. XRD ANALYSIS

The identification of Mg-Zn-Al-HT product samples was conducted by comparing 2θ values from the peaks of the synthesized compounds with a standards of the Joint Committee on Powder Diffraction Standard (JCPDS). The JCPDS standards used are Mg-Al hydrotalcite (JCPDS Number 89-0460) and Zn-Al hydrotalcite (JCPDS Number 38-0486). The diffraction patterns are presented in Fig. 1.

According to Rodriguez-Chiang et al., 2016 [32]; Ghashghae and Farzaneh (2018) [33], the main features of the HT were 2θ at 11, 23, 35, 39, 46, 61, and 62°. Based on the 2θ value, the fabricated Mg-Zn-Al-HT is in an agreement with Mg-Al-HT and Zn-Al-HT as reported by Valente et al., 2010 [34], and Elsayed et al., 2016 [2]. This proves that divalent ions (Mg^{2+} and Zn^{2+}) and trivalent (Al^{3+}) are the

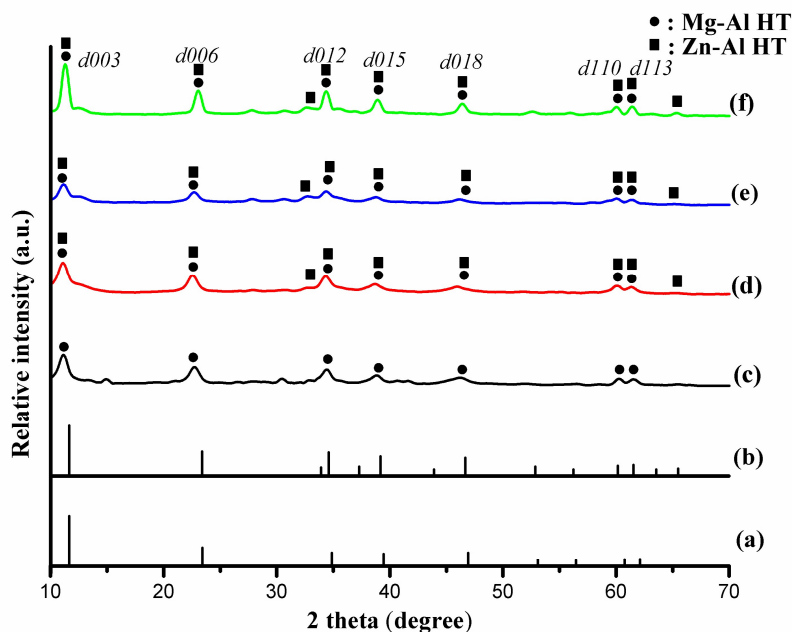


FIGURE 1. Diffractogram of (a) JCPDS Mg-Al-HT (b) JCPDS Zn-Al-HT (c) Mg-Al-HT (d) Mg-Zn1-Al HT (e) Mg-Zn2-Al HT (f) Mg-Zn3-Al HT.

constituent ions of Mg-Zn-Al-HT, which are bound in the HT layer together with the hydroxyl groups. In general, Mg-Zn-Al-HT is more likely to form a hydroxalite compound in which the divalent ions that play a role are Mg^{2+} ions. However, Zn^{2+} ions are also bound in the HT layer with the hydroxyl groups and trivalent ions. This was proven by the appearance of a peak that is similar to the peak of Zn-Al-HT. The Mg^{2+} and Zn^{2+} ions, which are bound to the HT layer, can undergo exchanges due to the similar atomic radius difference. The dimensions of the Mg^{2+} , Zn^{2+} , and Al^{3+} radii are 0.72 Å, 0.74 Å and 0.54 Å, respectively [5, 35]. According to Cavani et al., 1991 [1], divalent metal cations with radii between 0.3-0.9 Å and trivalent metal cations with radii of 0.5-0.8 Å will form a more regular octahedral coordination with the hydroxyl groups.

3.1.2. FTIR ANALYSIS

Figure 2 shows four FTIR Mg-Zn-Al-HT spectrums at various molar ratios.

Fig. 2 shows the absorption at wavenumbers between 3490-3457 cm^{-1} . That was identified as the absorption of O-H group (hydroxyl) stretching. The O-H group in the absorption is possible to come from a hydroxyl group that binds to M-OH or it comes from H_2O , which is bound to the interlayer anion. The absorption in wavenumbers between 1642-1506 cm^{-1} is the absorption of O-H groups bending that are possibly water molecules in the interlayer [2-5, 35, 36]. The FTIR spectra of Mg-Al-Zn-HT also shows the absorption of wavenumbers in the area of 1384-1381 cm^{-1} , which is a typical absorption of the C=O group (carbonyl) of CO_3^{2-} acting as an interlayer

balancing anion [2-5, 36]. The existence of divalent and trivalent metals in the structure of Mg-Zn-Al-HT can be seen with the appearance of the metal absorption bound to oxygen (M-O) at wavenumbers 414-835 cm^{-1} . Wavenumbers in the 783 cm^{-1} regions are the absorption of Al-O and Zn-Al-O at the hydroxalite layer. In addition, the absorption at wavenumbers 670-620 cm^{-1} is the absorption of C=O from carbonate vibrations, 590-560 cm^{-1} is the absorption of M-O, M-O-M, and O-M-O. While the absorption in wavenumbers 460-420 cm^{-1} is the absorption of Mg-OH, Al-OH, Zn-OH at the hydroxalite layer in the octahedral coordination [5].

3.1.3. Mg-Zn-Al HT OPTIMIZATION

The effect of Zn^{2+} addition to the Pb^{2+} adsorption is shown in Fig. 3.

In accordance with Fig. 3, it is known that the addition of Zn^{2+} is directly proportional to the Pb^{2+} ions adsorption efficiency. The efficiency of the Pb^{2+} adsorption on Mg-Zn1-Al HT with a molar ratio of 3 : 1 : 1 is only 73.16%. However, the efficiency of the Pb^{2+} adsorption to Mg-Zn-Al HT with a molar ratio of 2 : 2 : 1 and 1 : 3 : 1 does not increase significantly. The Mg-Zn2-Al HT adsorbent has an adsorption efficiency of 75.48%, while the Mg-Zn3-Al HT has an adsorption efficiency of 77.41%. Therefore, for the optimization of the effect of adding Zn^{2+} on the adsorbent, Mg-Zn-Al HT was chosen with a 3 : 1 : 1 molar ratio. Even with a small Zn^{2+} molar ratio, it has been able to increase the adsorption ability almost equal the addition of a larger number of moles. The increase of Zn^{2+} addition causes the surface of Mg-Zn-Al HT become more positively charged and

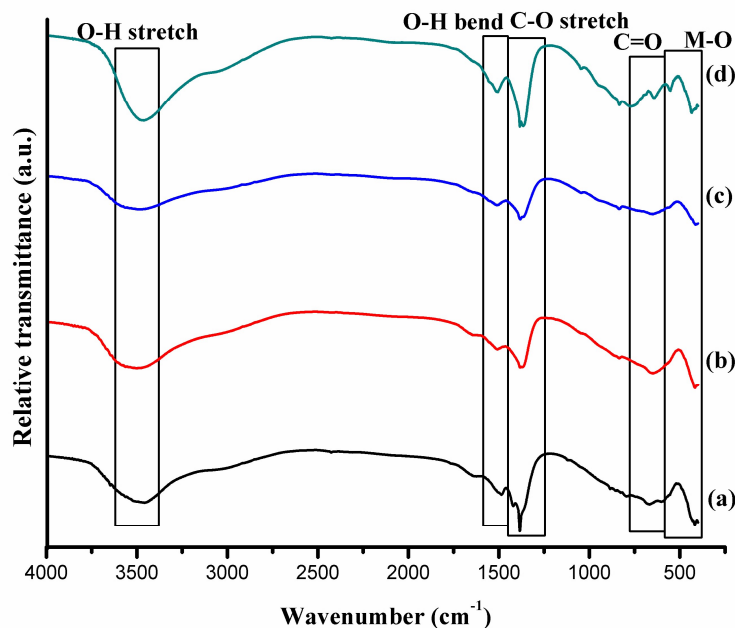


FIGURE 2. FTIR spectra of (a) Mg-Al-HT, (b) Mg-Al-Zn1-HT, (c) Mg-Al-Zn2-HT, (d) Mg-Al-Zn3-HT.

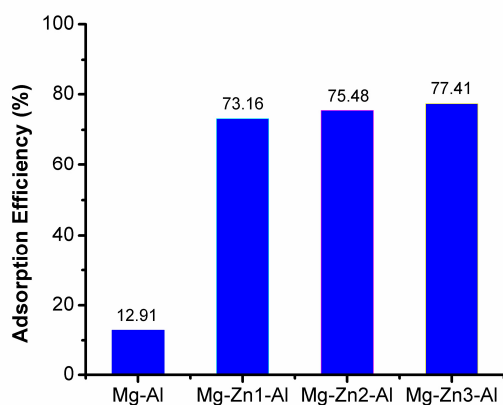


FIGURE 3. The effect of Zn^{2+} addition on the structure of Mg-Al HT on Pb^{2+} metal ions adsorption.

it will attract more hydroxide ions. Along with this, the hydroxide ion will attract Pb^{2+} which will form $Pb(OH)_2$.

3.1.4. CHARACTERIZATION OF METAL OXIDE FORMATION FROM Mg-Zn-Al HT

The adsorbent of Mg-Zn-Al HT and its oxides were characterized by the XRD to determine the effect of calcination on the formation of Mg-Zn-Al HT oxide. The XRD diffractogram of Mg-Zn-Al HT and its oxides is shown in Fig. 4.

It can be seen, in Fig. 4, that the calcination causes the intensity of the HT peak to decrease and also forms a new peak, namely MgO (JCPDS No.78-0430) and ZnO (JCPDS No.89-1397). The calcination treat-

ment at $450^\circ C$ causes a loss of water molecules and carbonate ions in the interlayer due to the damage of Mg-Zn-Al HT structure. The FTIR spectrum of Mg-Zn-Al HT and Mg-Zn-Al HT oxides are shown in Fig. 5.

Based on Fig. 5, it can be seen that there is an absorption at the wavenumber $3525-3490\text{ cm}^{-1}$ which is identified as the absorption of O-H group stretch. The stretched O-H group is probably coming from hydroxyl groups, which bind to divalent and trivalent cation metals in the layer or can also be possible from H_2O present in the interlayer [2, 5]. The absorption in the wavenumber $1607-1527\text{ cm}^{-1}$ is the absorption of the O-H group bending of water molecules in the interlayer. A typical absorption of the C-O group (carbonyl) of CO_3^{2-} , which is the interlayer balancing anion, is shown by the absorption at wavenumbers $1384-1381\text{ cm}^{-1}$. The absorption of C=O from carbonate vibrations is shown by the absorption at wavenumbers $648-636\text{ cm}^{-1}$. Absorption at wavenumbers $460-420\text{ cm}^{-1}$ is the absorption of Mg-OH, Al-OH, Zn-OH at the hydrotalcite layer in the octahedral coordination [5].

3.2. EFFECTIVENESS TEST OF Mg-Zn-Al HT AND ITS OXIDE TO Pb^{2+} ADSORPTION

The test results of the adsorption effectiveness of Mg-Zn-Al HT and its oxidized form for Pb^{2+} removal are shown in Fig. 6.

As seen in Fig. 6, it appears that the adsorption ability of Mg-Zn-Al HT oxide on Pb^{2+} metal is higher than that of Mg-Zn-Al HT. The high adsorption ability of Mg-Zn-Al HT oxide due to the calcination treatment could disperse the metal cations in the layer

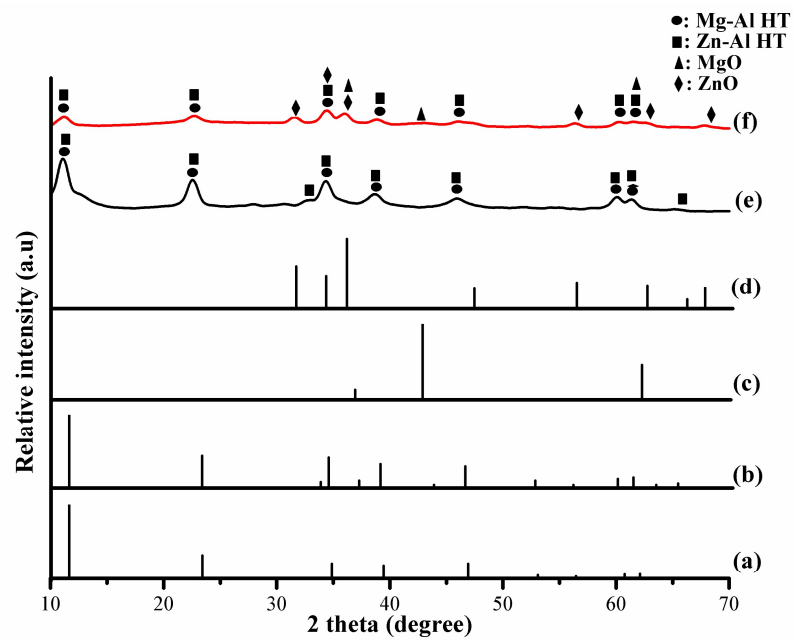


FIGURE 4. The diffractogram of (a) JCPDS Mg-Al HT (b) JCPDS Zn-Al HT (c) JCPDS MgO (d) JCPDS ZnO (e) Mg-Zn-Al HT and (f) Mg-Zn-Al HT oxide.

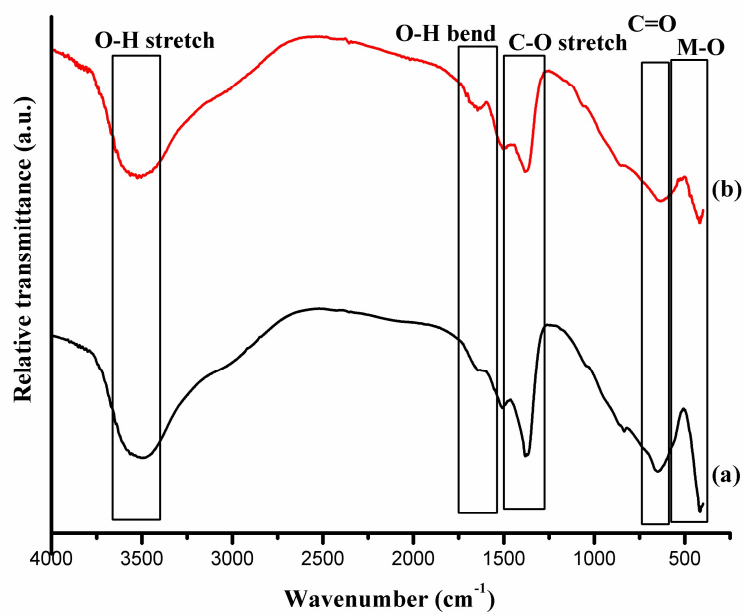


FIGURE 5. The FTIR spectrum of (a) Mg-Zn-Al HT and (b) Mg-Zn-Al HT oxide.

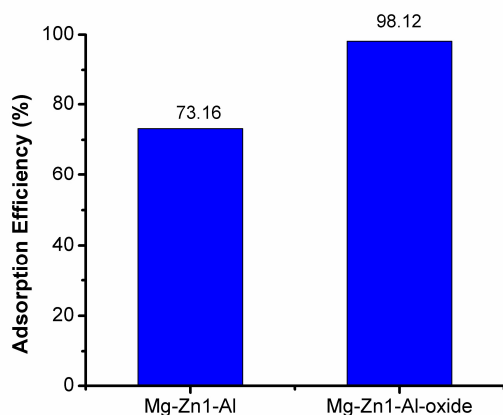


FIGURE 6. Adsorption efficiency of Mg-Zn1-Al HT and Mg-Zn1-Al HT oxide to Pb^{2+} metal ion.

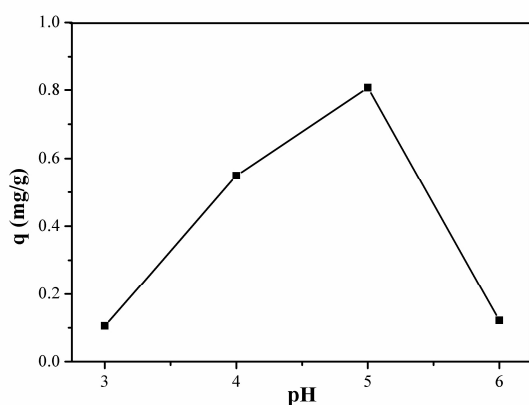


FIGURE 7. Effect of pH on Pb^{2+} metal adsorption efficiency.

homogeneously. As a result, the O – H group on the layer is evenly distributed on the entire surface of the Mg-Zn-Al oxide, which can then precipitate Pb^{2+} more effectively on the surface of the layer as $Pb(OH)_2$. In addition, the structure regeneration of Mg-Zn-Al HT when dispersed into the water-known as the ‘memory effect’ tends to attract hydroxide ions on the surface of the positively charged Mg-Zn-Al HT layer so that it can precipitate metal on the surface of Mg-Zn-Al HT [2, 11].

3.3. ADSORPTION STUDIES OF Pb^{2+} USING Mg-Zn-Al HT OXIDE

3.3.1. OPTIMUM pH DETERMINATION OF $Pb(NO_3)_2$ SOLUTION

The pH variations were 3, 4, 5, and 6. The effect of the pH variation on the Pb^{2+} ions adsorption efficiency is shown in Fig 7.

According to Fig. 7, it can be seen that the optimum pH condition is achieved at pH 5. Similar results have been reported in previous studies by Yang et al., 2016 [3] that determined the optimum pH of $Pb(NO_3)_2$ to

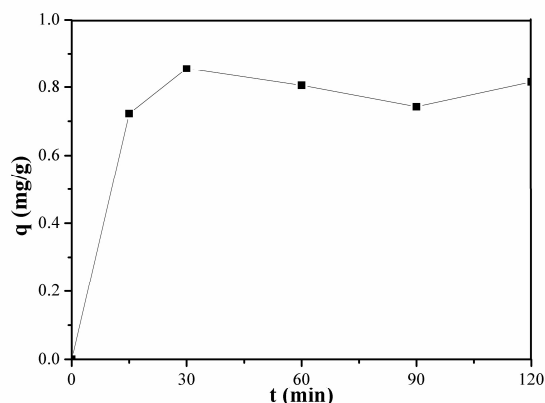


FIGURE 8. Effect of contact time on Pb^{2+} metal adsorption efficiency.

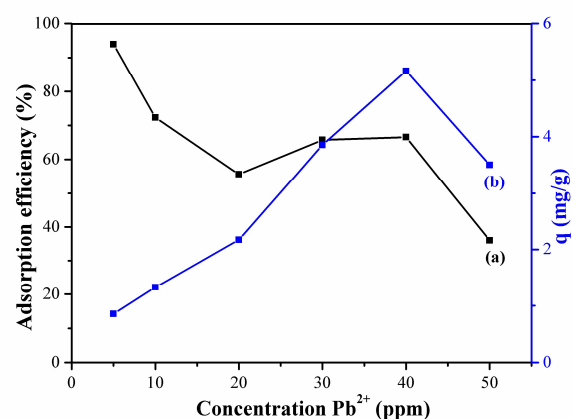


FIGURE 9. Effect of initial concentration on Pb^{2+} metal adsorption on (a) adsorption efficiency and (b) adsorption capacity.

be at pH 5. The adsorption efficiency of Pb^{2+} ion at pH 5 is 92.23% with an adsorption capacity of 0.81 mg/g. At pH 3, the adsorption efficiency only reached 10.83% and at pH above 5, the adsorption efficiency decreases.

3.3.2. EFFECT OF CONTACT TIME

The profile of the contact time variation effect to the Pb^{2+} adsorption efficiency is illustrated as shown in Fig. 8.

Under certain conditions, based on Fig. 8, the adsorption percentage decreases and then becomes constant. The optimum contact time is 30 minutes with an adsorption efficiency of 93.88% and an adsorption capacity of 0.86 mg/g.

3.3.3. EFFECT OF INITIAL CONCENTRATION

The effect of the initial concentration on the Pb^{2+} adsorption was carried out at concentrations of 5, 10, 20, 30, 40, and 50 ppm. The profile of the effect of the

initial concentration on the efficiency and adsorption capacity is presented in Fig. 9.

It is known that the initial concentration of $\text{Pb}(\text{NO}_3)_2$ solution is inversely proportional to the adsorption ability. Fig. 9(a) shows that the decrease in adsorption efficiency occurs as the initial concentration of Pb^{2+} increases. According to Elsayed et al., 2016 [2], the decreasing of the adsorption efficiency occurs at higher concentrations; the amount of Pb^{2+} ions in solution is not proportional to the number of available adsorbent particles. Hence, the surface of the adsorbent will reach a saturation point and then the adsorption efficiency will decrease. While Figure 9(b) shows that the increasing of the adsorbed- Pb^{2+} per gram adsorbent is proportional to the initial concentration of Pb^{2+} solution. When the adsorbate concentration increases, more molecules are adsorbed per unit surface area of the adsorbent. The increasing concentration of Pb^{2+} will give the thrust of Pb^{2+} ions to be adsorbed in the adsorbent pores [37].

3.3.4. CHARACTERIZATION OF Mg-Zn-Al HT OXIDE ADSORBENT AFTER Pb^{2+} ADSORPTION

The characterization of the Mg-Zn-Al HT oxide adsorbent after the Pb^{2+} adsorption process was conducted with the FTIR and XRD. The functional group of Mg-Zn-Al HT oxide adsorbent before and after the Pb^{2+} adsorption are shown in Fig. 10.

Figure 10 shows an absorption of O – H group stretching at a wavenumber of 3525 cm^{-1} , in the Mg-Zn-Al HT before the adsorption. The similar peak appears at 3480 cm^{-1} in the Mg-Zn-Al HT after the adsorption. Meanwhile, the absorption of O – H groups bending from H_2O molecules in the interlayer before adsorption at wavenumbers of 1527 cm^{-1} and after the adsorption at 1575 cm^{-1} . The typical absorption of the C – O group (carbonyl) of CO_3^{2-} that is the interlayer balancing anion before the adsorption is shown at 1381 cm^{-1} and after the adsorption, it is shown at 1379 cm^{-1} . The absorption of C=O from carbonate vibrations is shown by absorption at $636\text{--}610\text{ cm}^{-1}$. Absorption at $460\text{--}420\text{ cm}^{-1}$ is the absorption of Mg-OH, Al-OH, Zn-OH on the hydrotalcite layer in octahedral coordination [5].

The diffractogram of Mg-Zn-Al HT oxide before and after the adsorption is shown in Fig. 11.

Based on Fig. 11, it can be seen that the peak of metal oxides, such as MgO and ZnO, formed by the calcination treatment is not formed again after the adsorption process. The intensity of typical HT peaks also increases after the adsorption process due to the nature of the memory effect on the HT. The structure reverts back to the initial Mg-Zn-Al HT structure after being dispersed in a solution.

The elemental composition of Mg-Zn-Al HT oxide adsorbent before and after the adsorption of Pb^{2+} ions was analysed by Scanning Electron Microscopy-Energy Dispersive X-Ray (SEM-EDX). Each element's

percentage in the Mg-Zn-Al HT oxide is presented in Table 1.

According to the data in Table 1, it can be seen that Pb is present in the Mg-Zn-Al HT oxide after the adsorption. It proves that the Pb^{2+} ions were adsorbed onto it. The morphology of Mg-Zn-Al HT oxide adsorbent before and after the Pb^{2+} adsorption process was characterized by the SEM, and the result is depicted in Fig. 12.

Figure 12(a) shows that on the surface of the Mg-Zn-Al HT oxide adsorbent, there are hollow holes with different shapes and sizes, while Fig. 12(b) indicates the adsorbent surface tends to be coarser with more closed holes. The closed-holes indicate that the holes were filled with the Pb^{2+} adsorbed on the surface of Mg-Zn-Al HT oxide during the adsorption. Similar result had been reported by Mostafa et al., 2016 [12] in his study using Co-Mo hydrotalcite adsorbents.

3.4. DETERMINATION OF ADSORPTION KINETICS

The kinetic models used in this study are a pseudo first order (3) and pseudo second order (4) kinetics models [3].

$$\log(q_e - q_t) = \log q_e - \frac{k_1}{2.303}t \quad (3)$$

where q_e is the quantity of the solute adsorbed at an equilibrium per weight unit of adsorbent (mg/g), q_t is the quantity of the solute adsorbed at any time (mg/g), and k_1 is the sorption constant. For the pseudo-second-order model, the kinetic data were examined using a formula shown below:

$$\frac{1}{q_t} = \frac{1}{k_2 q_e^2} + \frac{1}{q_t} \quad (4)$$

where k_2 (g/(mg·min)) is the pseudo-second-order rate constant; t (min) is the sorption time; q_e (mg/g) is the equilibrium Pb^{2+} adsorption capacity of the adsorbent, and q_t (mg/g) is the sorption capacity at a time t .

Figure 13 shows the kinetic curve of the Mg-Zn-Al HT oxide adsorption on Pb^{2+} metal. A comparison of adsorption kinetics parameters is presented in Table 2.

Based on the adsorption kinetics parameter data presented in Table 2, it can be seen that the adsorption of Pb^{2+} using Mg-Zn-Al HT oxide tends to follow the pseudo second order equation. It is proved by the R^2 value for the pseudo second order, which is closer to one. The pseudo second order adsorption kinetics indicate that the adsorption occurs chemically. A research conducted on Pb^{2+} adsorption using the HT tends to follow a pseudo second order as in the study of Mostafa et al., 2016 [12] using Co-Mo HT and Yang et al., 2016 [3] using modified Mg-Al HT palygorskite.

3.5. DETERMINATION OF ADSORPTION ISOTHERM

The type of the adsorption is obtained by plotting the adsorption data based on the Langmuir and Fre-

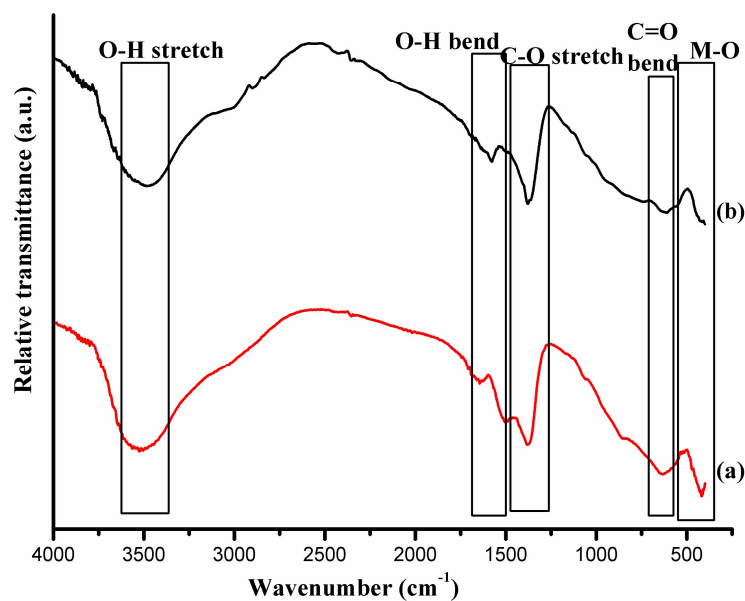


FIGURE 10. The functional group of Mg-Zn-Al HT oxide adsorbent (a) before and (b) after adsorption.

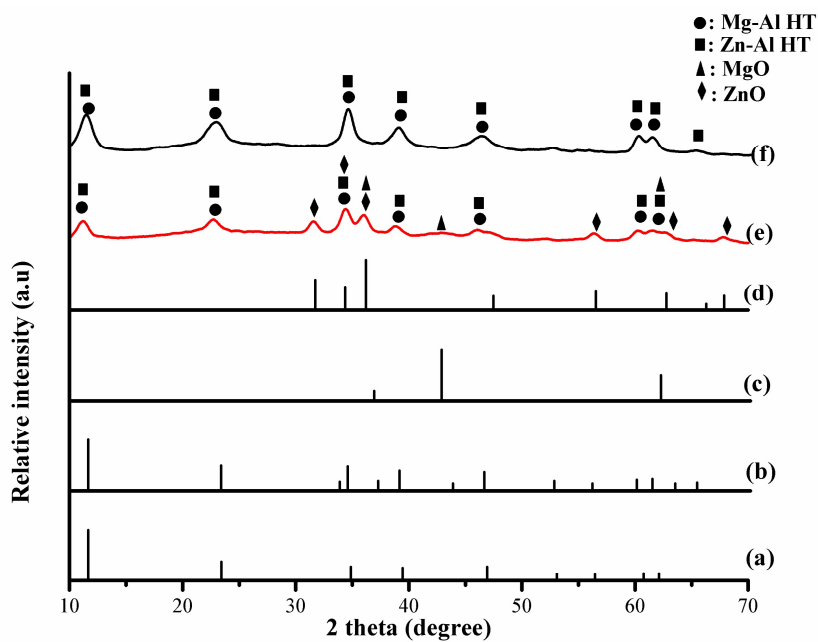


FIGURE 11. Diffractogram of (a) JCPDS Mg-Al HT (b) JCPDS Zn-Al HT (c) JCPDS MgO (d) JCPDS ZnO (e) Mg-Zn-Al HT oxide before adsorption and (f) Mg-Zn-Al HT oxide after adsorption.

Adsorption process	Element (%)					
	C	O	Mg	Al	Zn	Pb
Before	-	34.50	27.36	11.10	27.04	-
After	37.11	24.74	16.27	10.00	20.60	1.27

TABLE 1. The EDX result of Mg-Zn-Al HT before and after adsorption.

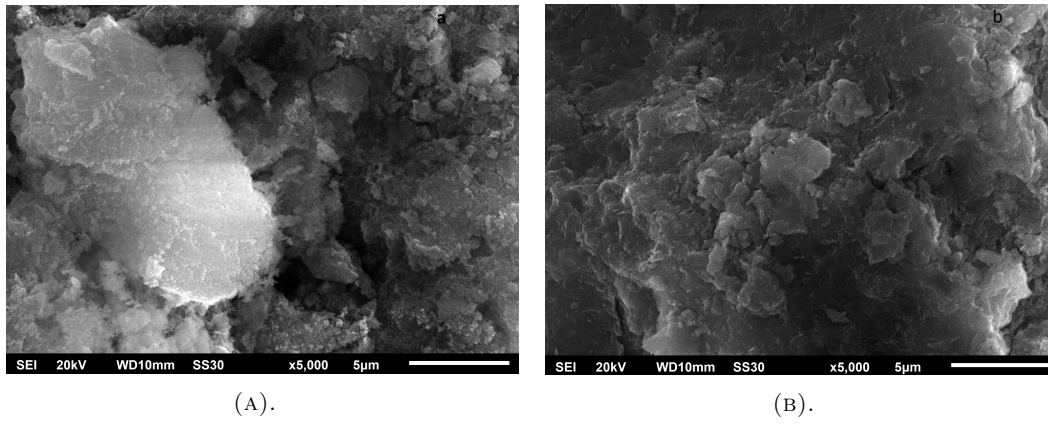


FIGURE 12. Morphology of Mg-Zn-Al HT (a) before and (b) after adsorption.

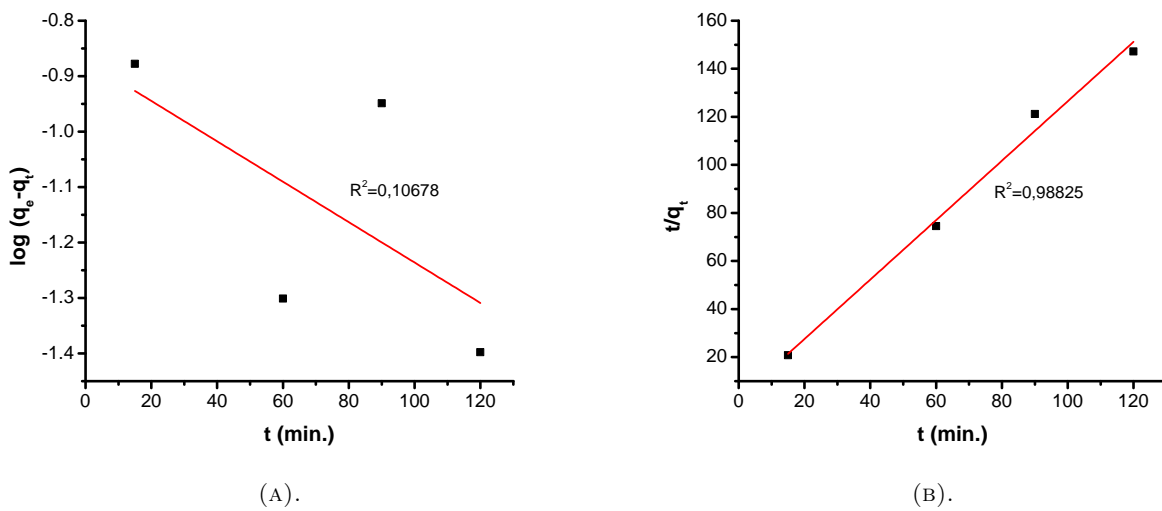


FIGURE 13. Adsorption kinetics curve of (a) pseudo first order and (b) pseudo second order.

Pseudo-first-order			Pseudo-double-order		
k_1 (1/min)	q_e (mg/g)	R^2	k_2 (g/mg·min)	q_e (mg/g)	R^2
0.0084	0.134	0.405	0.544	0.809	0.988

TABLE 2. Pseudo-first and pseudo-second-order models for the sorption of Pb^{2+} ions onto Mg-Zn-Al HT oxide.

Freundlich			Langmuir			
K_F (mg/g)	n	R^2	K_L (L/mmol)	E_a (kJ/mol)	R^2	Q_m (mg/g)
0.044	2.711	0.735	90.644	28.756	0.876	3.916

TABLE 3. Adsorption isotherm parameters for sorption of Pb^{2+} ions onto Mg-Zn-Al HT oxide.

Adsorbent	Adsorption capacity of Pb^{2+} (mg/g)	References
Cedar leaf ash	8.000	Hafshejani et al. [38]
Expanded perlite (EP)	13.390	Sari et al. [18]
Almond shells	4.500	Brudey et al. [39]
ZnO nanoparticles	6.700	Ma et al. [40]
Mg-Zn-Al HT	3.916	Present study

TABLE 4. The comparison of Pb^{2+} adsorption capacity on some adsorbent.

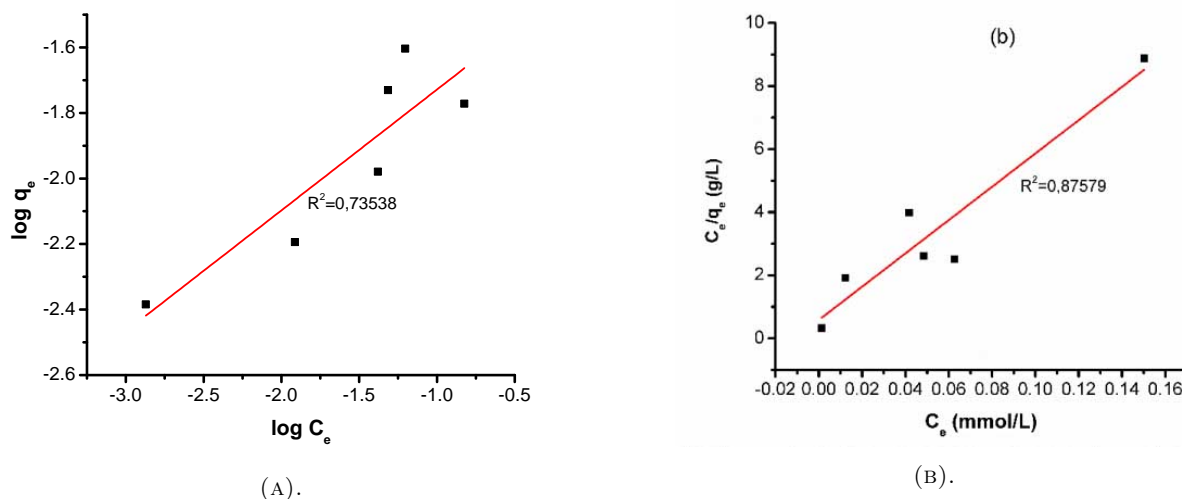


FIGURE 14. Adsorption isotherm curve of (a) Freundlich and (b) Langmuir.

undlich isotherm adsorption. The results are shown in Fig. 14. Meanwhile, the isotherm parameters are listed in Table 3.

Table 3 shows that the Pb^{2+} adsorption tends to follow the Langmuir isotherm with an adsorption capacity of 3.916 mg/g, the R^2 value is close to one. It indicates that the Pb^{2+} adsorption occurs due to a chemical bonding between the Pb^{2+} and hydroxide groups located on the surface of the Mg-Zn-Al HT oxide layer. The Langmuir isotherm model implies a homogeneous distribution of a single layer adsorbed molecules on the surface of the adsorbent. It is possibly caused by each hydroxide group as the active side on the surface of Mg-Zn-Al HT only adsorbing one Pb^{2+} ion.

Table 4 portrays other adsorbents used for a Pb^{2+} removal from aqueous solutions. These results indicate that the studied adsorbent is not appropriate for a Pb^{2+} removal from an aqueous solution without any modifications.

4. CONCLUSION

The molar ratio variation of Mg-Zn-Al HT increases the positive charge of Mg-Zn-Al HT. The calcination also increase the adsorption effectivity of Pb^{2+} . The adsorption, whether to Mg-Zn-Al HT or Mg-Zn-Al HT oxide, follows a pseudo-second-order kinetics model. While the isotherm follows the Langmuir model with a maximum adsorption capacity of 3.916 mg/g at pH 5 and the optimum contact time is 30 min at a room temperature.

ACKNOWLEDGEMENTS

The authors thank to Sebelas Maret University (Universitas Sebelas Maret) for providing financial support on this work under the scheme of 'Hibah Mandatory PNPB UNS, 2019 Grant'.

REFERENCES

- [1] F. Cavani, F. Trifirò, A. Vaccari. Hydrotalcite-type anionic clays: Preparation, properties and applications. *Catalysis Today* **11**(2):173–301, 1991. DOI:10.1016/0920-5861(91)80068-K.
- [2] M. El-Sayed, G. Eshaq, A. E. ElMetwally. Adsorption of heavy metals from aqueous solutions by Mg-Al-Zn mingled oxides adsorbent. *Water Science and Technology* **74**:1644–1657, 2016. DOI:10.2166/wst.2016.329.
- [3] F. Yang, S. Sun, X. Chen, et al. Mg-Al layered double hydroxides modified clay adsorbents for efficient removal of Pb^{2+} , Cu^{2+} and Ni^{2+} from water. *Applied Clay Science* **123**:134–140, 2016. DOI:10.1016/j.clay.2016.01.026.
- [4] M. Ghashghaee, S. Shirvani, V. Farzaneh, S. Sadjadi. Hydrotalcite-impregnated copper and chromium-doped copper as novel and efficient catalysts for vapor-phase hydrogenation of furfural: Effect of clay pretreatment. *Brazilian Journal of Chemical Engineering* **35**:669–678, 2018. DOI:10.1590/0104-6632.20180352s20160703.
- [5] L. Cochechi, P. Barvinschi, R. Pode, et al. Structural characterization of some Mg/Zn-Al type hydrotalcites prepared for chromate sorption from wastewater. *Chemical Bulletin of POLITEHNICA University of Timisoara* **55**:40–45, 2010.
- [6] T. Kameda, T. Yoshioka, K. Watanabe, et al. Dehydrochlorination behavior of a chloride ion-intercalated hydrotalcite-like compound during thermal decomposition. *Applied Clay Science* **35**:173–179, 2007. DOI:10.1016/j.clay.2006.08.010.
- [7] M. Bouraada, F. Belhafaoui, M. S. Ouali, L. De Ménorval. Sorption study of an acid dye from an aqueous solution on modified Mg-Al layered double hydroxides. *Journal of Hazardous Materials* **163**:463–467, 2009. DOI:10.1016/j.jhazmat.2008.06.108.
- [8] K. Abderrazek, F. Srasra Najoua, E. Srasra. Synthesis and characterization of [Zn-Al] LDH: Study of the effect of calcination on the photocatalytic activity. *Applied Clay Science* **119**:229–235, 2016. DOI:10.1016/j.clay.2015.10.014.

- [9] M. Jenisha Barnabas, S. Parambadath, A. Mathew, et al. Highly efficient and selective adsorption of In^{3+} on pristine Zn/Al layered double hydroxide (Zn/Al-LDH) from aqueous solutions. *Journal of Solid State Chemistry* **233**:133–142, 2016. DOI:10.1016/j.jssc.2015.10.001.
- [10] W. Wang, J. Zhou, G. Achari, et al. Cr(VI) removal from aqueous solutions by hydrothermal synthetic layered double hydroxides: Adsorption performance, coexisting anions and regeneration studies. *Colloids and Surfaces A: Physicochemical and Engineering Aspects* **457**:33–40, 2014. DOI:10.1016/j.colsurfa.2014.05.034.
- [11] A. A. Bakr, G. Eshaq, A. M. Rabie, et al. Copper ions removal from aqueous solutions by novel Ca–Al–Zn layered double hydroxides. *Desalination and Water Treatment* **57**(27):12632–12643, 2016. DOI:10.1080/19443994.2015.1051126.
- [12] M. Mostafa, A.-S. A. Bakr, A. El Naggar, E.-S. A. Sultan. Water decontamination via the removal of Pb (II) using a new generation of highly energetic surface nano-material: Co(+2) Mo(+6) LDH. *Journal of colloid and interface science* **461**:261–272, 2015. DOI:10.1016/j.jcis.2015.08.060.
- [13] B. Hassiba, M. Bouraada, L. Charles Deménorval. Removal of indigo carmine and green bezanyl-F2B from water using calcined and uncalcined Zn/Al + Fe layered double hydroxide. *Journal of Water Reuse and Desalination* **7**:152–161, 2017. DOI:10.2166/wrd.2016.042.
- [14] A. M. Abu-Dief, M. M. Zikry. Adsorption of the heavy metal ions onto bio sorbents: A review. *International Journal of Nanomaterials and Chemistry* **4**:27–39, 2018. DOI:10.18576/ijnc/040301.
- [15] A. Sari, M. Tuzen. Kinetic and equilibrium studies of Pb(II) and Cd(II) removal from aqueous solution onto colemanite ore waste. *Desalination* **249**:260–266, 2009. DOI:10.1016/j.desal.2008.12.057.
- [16] M. Ghashghaee, V. Farzaneh. Removal of Cr(VI) species from aqueous solution by different nanoporous materials. *Iranian Journal of Toxicology* **10**:15–21, 2016. DOI:10.29252/araku.10.6.15.
- [17] F. Fu, Q. Wang. Removal of heavy metal ions from wastewaters: A review. *Journal of environmental management* **92**:407–418, 2011. DOI:10.1016/j.jenvman.2010.11.011.
- [18] A. Sari, M. Tuzen, D. Çitak, M. Soylak. Adsorption characteristics of Cu(II) and Pb(II) onto expanded perlite from aqueous solution. *Journal of Hazardous Materials* **148**:387–394, 2007. DOI:10.1016/j.jhazmat.2007.02.052.
- [19] K. Yang, L.-g. Yan, Y.-m. Yang, et al. Adsorptive removal of phosphate by Mg–Al and Zn–Al layered double hydroxides: Kinetics, isotherms and mechanisms. *Separation and Purification Technology* **124**:36–42, 2014. DOI:10.1016/j.seppur.2013.12.042.
- [20] E. Herald, W. W. Lestari, D. Permatasari, D. D. Arimurti. Biosorbent from tomato waste and apple juice residue for lead removal. *Journal of Environmental Chemical Engineering* **6**:1201–1208, 2018. DOI:10.1016/j.jece.2017.12.026.
- [21] K. Jiang, T.-H. Sun, N. Sun, H.-B. Li. Adsorption characteristics of copper, lead, zinc and cadmium ions by tourmaline. *Journal of environmental sciences (China)* **18**:1221–1225, 2006. DOI:10.1016/S1001-0742(06)60066-1.
- [22] A. Azzam, S. El-Wakeel, B. B. Mostafa, M. F. El-Shahat. Removal of Pb, Cd, Cu and Ni from aqueous solution using nano scale zero valent iron particles. *Journal of Environmental Chemical Engineering* **4**:2196–2206, 2016. DOI:10.1016/j.jece.2016.03.048.
- [23] L. Monser, N. Adhoum. Tartrazine modified activated carbon for the removal of Pb(II), Cd(II) and Cr(III). *Journal of Hazardous Materials* **161**:263–269, 2009. DOI:10.1016/j.jhazmat.2008.03.120.
- [24] U. Wingenfelder, C. Hansen, G. Furrer, R. Schulin. Removal of heavy metals from mine waters by natural zeolites. *Environmental Science & Technology* **39**:4606–4613, 2005. DOI:10.1021/es048482s.
- [25] J. Perić, M. Trgo, N. V. Medvidović. Removal of zinc, copper and lead by natural zeolite — a comparison of adsorption isotherms. *Water Research* **38**:1893–1899, 2004. DOI:10.1016/j.watres.2003.12.035.
- [26] M. Ghashghaee, M. Ghambarian. Adsorption of toxic mercury, lead, cadmium, and arsenic ions on black phosphorous nanosheet: first-principles calculations. *Structural Chemistry* **30**:85–96, 2018. DOI:10.1007/s11224-018-1173-6.
- [27] M. Madhava Rao, D. Ramana, K. Seshaiah, et al. Removal of some metal ions by activated carbon prepared from Phaseolus aureus hulls. *Journal of Hazardous Materials* **166**:1006–1013, 2009. DOI:10.1016/j.jhazmat.2008.12.002.
- [28] X. Li, J. Xing, C. Zhang, et al. Adsorption of lead on sulfur-doped graphitic carbon nitride nanosheets: Experimental and theoretical calculation study. *ACS Sustainable Chemistry & Engineering* **6**:10606–10615, 2018. DOI:10.1021/acssuschemeng.8b01934.
- [29] S. Basahel, S. Al-Thabaiti, N. Katabathini, et al. Nanostructured Mg–Al hydrotalcite as catalyst for fine chemical synthesis. *Journal of Nanoscience and Nanotechnology* **14**:1931–1946, 2014. DOI:10.1166/jnn.2014.9193.
- [30] L. Abdel-Rahman, A. Abu-Dief, M. A. Abd-El Sayed, M. M. Zikry. Nano sized moringa oleifera an effective strategy for Pb(II) ions removal from aqueous solution. *Chemistry and Materials Research* **8**:8–22, 2016.
- [31] L. Abdel-Rahman, A. Abudief, B. S. F. Al-Farhan, M. M. Zikry. Removal of toxic Pb(II) ions from aqueous solution by nano sized flamboyant pod (Delonix regia). *Archives in Chemical Research* **01**:1–10, 2016. DOI:10.21767/2572-4657.100003.
- [32] L. Rodriguez-Chiang, J. Llorca, O. Dahl. Effect of Fe–Zn–Mg–Al hydrotalcites on the methane potential of synthetic sulfate-containing wastewater. *Journal of Water Process Engineering* **10**:120–127, 2016. DOI:10.1016/j.jwpe.2016.03.001.
- [33] M. Ghashghaee, V. Farzaneh. Nanostructured hydrotalcite-supported RuBaK catalyst for direct conversion of ethylene to propylene. *Russian Journal of Applied Chemistry* **91**:972–976, 2018. DOI:10.1134/S1070427218060149.

- [34] J. Valente, J. Hernández-Cortez, M. Sánchez-Cantú, et al. Calcined layered double hydroxides Mg–Me–Al (Me: Cu, Fe, Ni, Zn) as bifunctional catalysts. *Catalysis Today* **150**:340–345, 2010. DOI:10.1016/j.cattod.2009.08.020.
- [35] K. Abou-El-Sherbini, I. M. Kenawy, M. A. Hafez, et al. Synthesis of novel CO₃²⁻/Cl⁻-bearing 3(Mg+Zn)/(Al+Fe) layered double hydroxides for the removal of anionic hazards. *Journal of Environmental Chemical Engineering* **3**:2707–2721, 2015. DOI:10.1016/j.jece.2015.09.015.
- [36] E. Herald, S. Santosa, Triyono, K. Wijaya. Anionic and cationic dyes removal from aqueous solutions by adsorption onto synthetic Mg/Al hydrotalcite-like compound. *Indonesian Journal of Chemistry* **2015**:234–241, 2015. DOI:10.22146/ijc.21190.
- [37] L. Wu, L. Melton, L. Sanguansri, M. A. Augustin. The batch adsorption of the epigallocatechin gallate onto apple pomace. *Food Chemistry* **160**:260–265, 2014. DOI:10.1016/j.foodchem.2014.03.098.
- [38] L. Divband Hafshejani, S. Nasab, R. Mafi Gholami, et al. Removal of zinc and lead from aqueous solution by nanostructured cedar leaf ash as biosorbent. *Journal of Molecular Liquids* **211**:448–456, 2015. DOI:10.1016/j.molliq.2015.07.044.
- [39] T. Brudey, L. Largitte, C. Jean-Marius, et al. Adsorption of lead by chemically activated carbons from three lignocellulosic precursors. *Journal of Analytical and Applied Pyrolysis* **120**:450–463, 2016. DOI:10.1016/j.jaap.2016.06.018.
- [40] M. Xingfa, Y. Wang, M. Gao, et al. A novel strategy to prepare ZnO/PbS heterostructured functional nanocomposite utilizing the surface adsorption property of ZnO nanosheets. *Catalysis Today* **158**:459–463, 2010. DOI:10.1016/j.cattod.2010.07.013.